Terr. Atmos. Ocean. Sci., Vol. 25, No. 3, 449-461, June 2014 doi: 10.3319/TAO.2014.01.02.01(Hy)

Tsengwen Reservoir Watershed Hydrological Flood Simulation Under Global Climate Change Using the 20 km Mesh Meteorological Research Institute Atmospheric General Circulation Model (MRI-AGCM)

Nobuaki Kimura, Shen Chiang *, Hsiao-Ping Wei, Yuan-Fong Su, Jung-Lien Chu, Chao-Tzuen Cheng, Jun-Jih Liou, Yung-Ming Chen, and Lee-Yaw Lin

National Science and Technology Center for Disaster Reduction (NCDR), New Taipei City, Taiwan

Received 25 January 2013, accepted 2 January 2014

ABSTRACT

Severe rainstorms have occurred more frequently in Taiwan over the last decade. To understand the flood characteristics of a local region under climate change, a hydrological model simulation was conducted for the Tsengwen Reservoir watershed. The model employed was the Integrated Flood Analysis System (IFAS), which has a conceptual, distributed rainfall-runoff analysis module and a GIS data-input function. The high-resolution rainfall data for flood simulation was categorized into three terms: 1979 - 2003 (Present), 2015 - 2039 (Near-future), and 2075 - 2099 (Future), provided by the Meteorological Research Institute atmospheric general circulation model (MRI-AGCM). Ten extreme rainfall (top ten) events were selected for each term in descending order of total precipitation volume. Due to the small watershed area the MRI-AGCM3.2S data was downsized into higher resolution data using the Weather Research and Forecasting Model. The simulated discharges revealed that most of the Near-future and Future peaks caused by extreme rainfall increased compared to the Present peak. These ratios were 0.8 - 1.6 (Near-future/Present) and 0.9 - 2.2 (Future/Present), respectively. Additionally, we evaluated how these future discharges would affect the reservoir's flood control capacity, specifically the excess water volume required to be stored while maintaining dam releases up to the dam's spillway capacity or the discharge peak design for flood prevention. The results for the top ten events show that the excess water for the Future term exceeded the reservoir's flood control capacity and was approximately 79.6 - 87.5% of the total reservoir maximum capacity for the discharge peak design scenario.

Key words: IFAS, High-resolution MRI-AGCM3.2S, Flood simulation, Tsengwen Reservoir watershed, Global climate change

Citation: Kimura, N., S. Chiang, H. P. Wei, Y. F. Su, J. L. Chu, C. T. Cheng, J. J. Liou, Y. M. Chen, and L. Y. Lin, 2014: Tsengwen Reservoir watershed hydrological flood simulation under global climate change using the 20 km mesh Meteorological Research Institute atmospheric general circulation model (MRI-AGCM). Terr. Atmos. Ocean. Sci., 25, 449-461, doi: 10.3319/TAO.2014.01.02.01(Hy)

1. INTRODUCTION

A flood-induced disaster kills people and damages properties. Severe flooding frequently occurs in Taiwan, located in the North Pacific subtropical region. Severe floods in Taiwan normally occur within a short-period of floodwater convergence (3 to 6 h) after a severe typhoon or due to heavy seasonal precipitation causing torrential stream flows down the steep mountains (Hsu et al. 2003). The average annual damage from past flooding events was approximately US $500 million year^{-1} (Yen et al. 1998). Flooding became more severe and occurred more often in the last decade according to the statistical analysis of disasters caused by heavy rainstorms for the time period between 1970 and 2009 (NCDR 2010; Hsu et al. 2011). For example, Typhoon Morakot (August 2009) killed more than 500 people and caused approximately $912 million (USD) in economic loss in Taiwan due to strong floods, debris flows and slope collapse (http://www.ncdr.nat.gov.tw/). According to a climate model prediction under global climate change scenarios over the next 100 years, global mean temperatures are expected to increase by 0.9° to 3.5°C and the sea level is likely to rise up to 1 m, compared to the air temperature and sea level in 1990 (Houghton et al. 1990, 1995). Moreover, the Bernstein et al. (2007) and Field et al. (2012) reported that frequent extreme weather events were evident globally over the last decade and concluded that global climate change would cause an

* *Corresponding author*
E-mail: johnson@ncdr.nat.gov.tw

increase in future extreme weather events such as super-typhoons and category-5 hurricanes. This conclusion implies that the typhoon- and seasonal rainfall-induced floods in the North Pacific region may become more destructive. It is therefore necessary to gain a better understanding of the trends and characteristics of river flooding in the years ahead to prevent or mitigate severe flood disasters.

The direct effects of global climate change on local extreme weather (e.g., typhoon and seasonal heavy rainfall) are being studied in the Taiwan Climate Change Projection and Information Platform Project (TCCIP). The TCCIP is investigating the impacts of local climate change on Taiwanese society (infrastructure, infectious disease, people's life style, etc.) developing an integrated platform in the form of a local climate change database which has been downscaled from global climate change applications (NCDR 2010). The extreme weather forecasts affected by local climate change were provided for three terms: Present (1979 - 2003), Near-future (2015 - 2039) and Future (2075 - 2099), using an atmospheric general circulation model (AGCM) for the entire globe produced by Meteorological Research Institute in Japan Meteorological Agency (JMA-MRI). Hereinafter, the JMA-MRI model is called MRI-AGCM. One of the goals in this project is to reveal how typhoon- and heavy rainfall-induced floods will change in the future under global climate change. In order to achieve this goal we implemented an existing hydrological model that is driven by the AGCM forecast rainfall data (high spatial and temporal resolution) to a specific local region in Taiwan.

This hydrological model can simulate unsteady discharge under flooding conditions. The development, calibration and validation of hydrological models using historical extreme weather-induced floods have been detailed in many studies (e.g., Wang and Xu 2011). However, these studies were conducted for a spatially large region and a temporally long period. In the case of Taiwan, no study has yet been completed using a spatially and temporally high resolution under climate change induced future extreme precipitation events.

The purposes of this study are, using a conceptual, distributed hydrological model implemented for the Tsengwen Reservoir watershed in Taiwan, (1) to verify the hydrological model for a past typhoon, (2) compare the discharge peaks for current and future severe floods caused by the top ten extreme rainfall events for each simulated term (Present, Near-future, or Future), which were projected by the AGCM with high spatial and temporal resolution, and (3) evaluate the effect of these floods on the reservoir capacity and dam outlet controls under future climate conditions.

2. METHOD

2.1 MRI-AGCM and WRF

Three terms: Present (1979 - 2003), Near-future (2015 - 2039), and Future (2075 - 2099), were analyzed to reveal the flood characteristics in terms of peak discharge and cumulative runoff volume as potentially affected by long-term climate change. The Asian-scale meteorological data for the three terms were provided by MRI-AGCM, whose resolution is 20 km horizontally and capable of representing tropical cyclones and extreme indices under the effect of climate change (Mizuta et al. 2006; Oouchi et al. 2006; Kitoh et al. 2008; Mizuta et al. 2012). As the lower boundary conditions for the Present, Near-future and Future terms, the MRI-AGCM incorporated the observed Sea Surface Temperature (SST) and ensemble SST projected from Phase 3 of the Coupled Model Inter-comparison Project dataset for the A1B IPCC scenario, which assumes global economic and population growth peak in mid-21st century and then decline (Mizuta et al. 2012). Note that the MRI-AGCM has two versions: MRI-AGCM3.1S and MRI-AGCM3.2S. We used the latter version in this study. Hereinafter, the data from MRI-AGCM3.2S is called MRI-data. For global climate projection downscaling to a regional climate scale we ran the Weather Research and Forecasting Model (WRF) with version 3.1.1, driven by the MRI data as the initial and boundary conditions, to simulate regional climate and obtain rainfall data with higher spatial and temporal resolutions. Five km horizontal resolution cells and 36 vertical layers, but no nested-grid treatment, were implemented in the WRF. The WRF employed several appropriate modules and schemes, such as Community Atmosphere Model for estimating radiation, Kain-Fritsch cumulus parameterization for resolving the cumulus clouds, Monin-Obukhov surface layer scheme for improving the surface layer formulation, Single-Moment 5-class Microphysics scheme for representing the rainfall fallout, condensation and thermodynamics effects. The YonSei University boundary scheme was used for treating the boundary layer of the vertical diffusion with a nonlocal turbulent mixing coefficient. The Noah land surface module was used for taking account of land-atmosphere interaction processes (see http://wrf-model.org/). In addition, the spectral nudging method was implemented to enforce the MRI-AGCM variables (i.e., wind velocity, temperature, and geo-potential height) above the planetary boundary layer to the WRF ones by minimizing the climate drift issue. The rainfall data computed by the WRF is supposed to capture more accurate topographical effects. The rainfall data with an hourly interval was bias-corrected using a statistical method that determines the tuning coefficient in order for the cumulative distribution function of the WRF-generated data to be close to that of the observed data with descending order (Piani et al. 2010). The bias-corrected data was used in the hydrological model. Hereinafter, the dynamic downscaled and biased-corrected data from MRI data are called MRI-WRF data.

2.2 Hydrological Model

To simulate river floods caused by typhoon and heavy

rainfall events, we utilized an integrated hydrological simulation system, the so-called Integrated Flood Analysis System (IFAS), which was developed by the International Centre for water Hazard and Risk Management (ICHARM) (Fukami et al. 2009; Sugiura et al. 2008). The IFAS has been practically applied to past flood events in Asian countries such as Japan (Sugiura et al. 2008) and Pakistan (Aziz and Tanaka 2011). The procedures to handle the IFAS are depicted in Fig. 1. A conceptual, distributed rainfall-runoff analysis engine, so-called Public Works Research Institute (PWRI)-distributed hydrological model (Yoshino et al. 1990), is employed in the IFAS. The IFAS has convenient interfaces for ground-based or satellite-based data rainfall input and has an input function for Geographic Information System (GIS)-based hydrological features, such as soil and geological types, land use, climatological zone and altitude. The first IFAS operation procedure creates a project name and sets up a target area. The GIS data for the hydrological information are imported into the IFAS and the basin shape and river course are then automatically generated using the differences in altitudes. The cell-type classification that indicates how water flows in upper, middle, and downstream areas is determined by the altitude difference and the distance from the origin of the water flow to a computational cell (Fig. 1). The rainfall data are also imported and the model parameters, as determined by the GIS-based hydrological features, are then set up. After pre-processing is complete the model is launched and the model output is obtained. In the final IFAS procedure a visualization of the outputs is combined with a virtual globe map and geographical information software (e.g., Google Earth). All procedures employ an interactive graphical user interface.

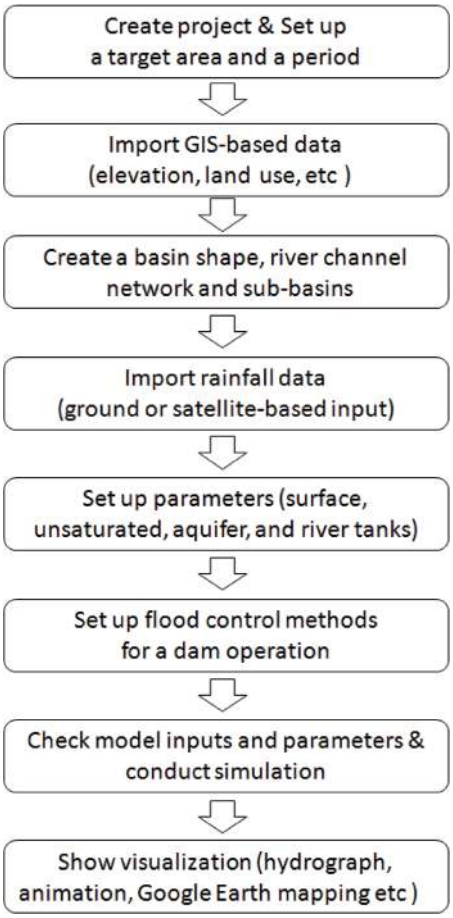

Fig. 1. Flowchart of the procedure for the IFAS operation.

The PWRI-distributed hydrological model divides the whole watershed into uniform cells and computes the flow at each cell. The flow is computed by surface, aquifer, and river tanks through two or three vertical layers (see Figs. 2 and 3). As depicted in Fig. 3 the three tanks are described in the following sentences. From the amount of precipitation, the surface tank (upper tank) provides the surface flow (Q_{sf}) ($m^3 s^{-1}$) (= cms), rapid intermediate outflow (Q_{ri}) (cms), and infiltration flow (Q_0) (cms) to the underground. The surface flow, described by Manning's formula, is proportional to stored water to the 5/3th power and is given by

$$Q_{sf} = \frac{\ell}{n}(h - S_{f2})^{5/3}\sqrt{I} \tag{1}$$

where h is the height of stored water (m), S_{f2} is the height (m) where Q_{sf} occurs (Maximum storage height), n is the equivalent roughness coefficient ($m^{-1/3}$ s) of the ground surface, ℓ is the length of cell (m), and I is the gradient of slope. The rapid intermediate and infiltration outflows are approximately proportional to the water stored in the soil and are respectively described by

$$Q_{ri} = \alpha_{ri} A f_0 (h - S_{f1})/(S_{f2} - S_{f1}) \tag{2}$$

where S_{f1} is the height (m) where Q_{ri} occurs, α_{ri} is the regulation coefficient for rapid intermediate flow, f_0 is the final infiltration capacity (ms^{-1}) and A is the area of cell (m^2), and

$$Q_0 = A f_0 (h - S_{f0})/(S_{f2} - S_{f1}) \tag{3}$$

where S_{f0} is the height (m) where Q_0 occurs. The Q_0 becomes the inflow of a lower layer. The relation among temporal deviation of the height, flows and rainfall in the surface tank is given by

$$\frac{\partial h}{\partial t} = \begin{cases} R - E_{ps} - Q_0 - Q_{sf} - Q_{ri} & S_{f2} \le h \\ R - E_{ps} - Q_0 - Q_{ri} & \text{if } S_{f1} \le h < S_{f2} \\ R - E_{ps} h/S_{f1} - Q_0 & S_{f0} \le h < S_{f1} \\ R - E_{ps} h/S_{f1} & h < S_{f0} \end{cases} \tag{4}$$

where R is the rainfall (m) and E_{ps} is the actual evapotranspiration (m), computed using the Penman-Monteith equation.

With the percolation inflow ($Q_{gin} = Q_0$) (cms) through the upstream surface, the groundwater tank (lower tank) calculates two outlet flows: unconfined groundwater flow (Q_{g1}) (cms) proportional to the second power of the water stored in the soil and confined groundwater flow (Q_{g2}) (cms) proportional to the water stored in the soil, given respectively by

$$Q_{g1} = \alpha_u^2 (h - S_g)^2 A$$
$$Q_{g2} = \alpha_g h A \quad (5)$$

where S_g is the height (m) where Q_{g1} occurs, and α_u ($m^{-1/2}\ s^{-1/2}$) and α_g (s^{-1}) are the regulation coefficient of slow intermediate outflow and coefficient of base-outflow, respectively. The relation among temporal deviation of the height, in- and out-flows in the groundwater tank is given by

$$\frac{\partial h}{\partial t} = \begin{cases} Q_{gin} - Q_{g1} - Q_{g2} & if \quad h \geq S_g \\ Q_{gin} - Q_{g2} & h < S_g \end{cases} \quad (6)$$

For the river tank, the flow of river channel (Q_r) (cms) is assumed to be governed by Manning's formula and is given by

$$Q_r = \frac{B}{n'} h^{5/3} \sqrt{i} \quad (7)$$

where B is the breadth of the channel (m), determined by two Resume Law constants ($B = c \cdot s$) , n' is the roughness coefficient of channel ($m^{-1/3}$ s), and i is the channel gradient. The relation among temporal deviation of the height, in- and out-flows is described as

$$LB \frac{\partial h}{\partial t} = Q_{rin} - Q_r \quad (8)$$

where Q_{rin} is the inflow (cms) through upstream surface and groundwater tanks, and L is the length of river channel (m). For the setup of physical-based parameters at each tank, all cells are categorized into several classification groups based upon the distance from upper stream and land use, geology and soil-type information. Each group has own values for the parameters. The default values for most parameters were calibrated by the past flood simulations (Sugiura et al. 2008).

In this study, the required IFAS input data for hydrological information were the elevation, land use, and soil-geology data. The elevation data was obtained from the Digital Elevation Model from the shuttle radar topography mission with three arc-second resolution, or about 90 m (downloaded from HydroSHEDS, see http://gisdata.usgs.gov/website/HydroSHEDS/). The land use data with 30 arc-second (~1 km) resolution was downloaded from Global Map data managed by the International Steering Committee for Global Mapping (http://iscgm.org/cgi-bin/fswiki/wiki.cgi). The data for the geology and soil type was obtained from the global distribution data for soil water holding capacity with one-degree resolution at 0 - 0.3 m from the United Nations Environment Program (http://www.grid.unep.ch/data/data.php). The

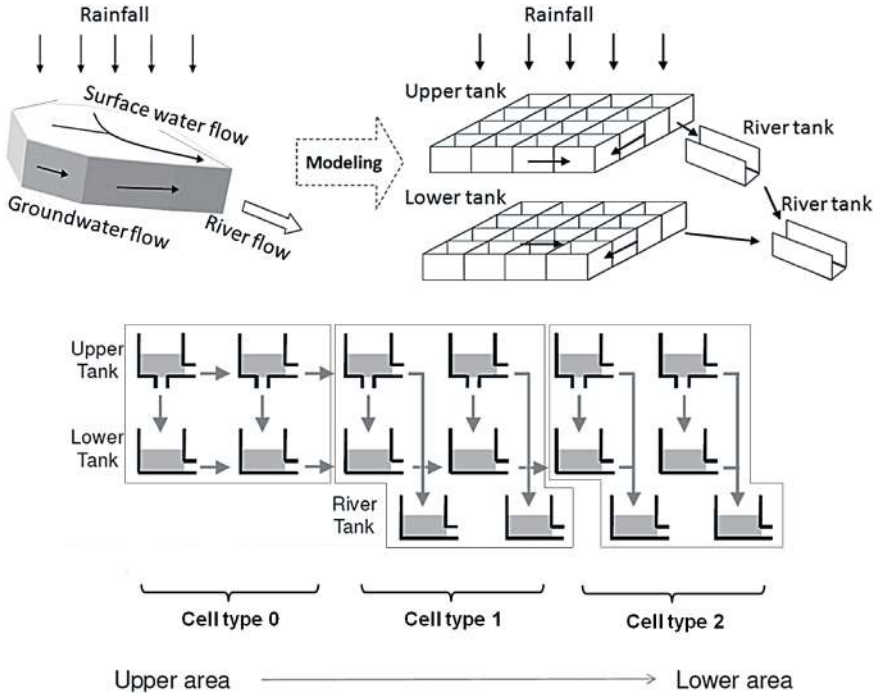

Fig. 2. Schematic diagram of the PWRI-distributed hydrological model, showing modeling (upper row) and flows in cells (lower row).

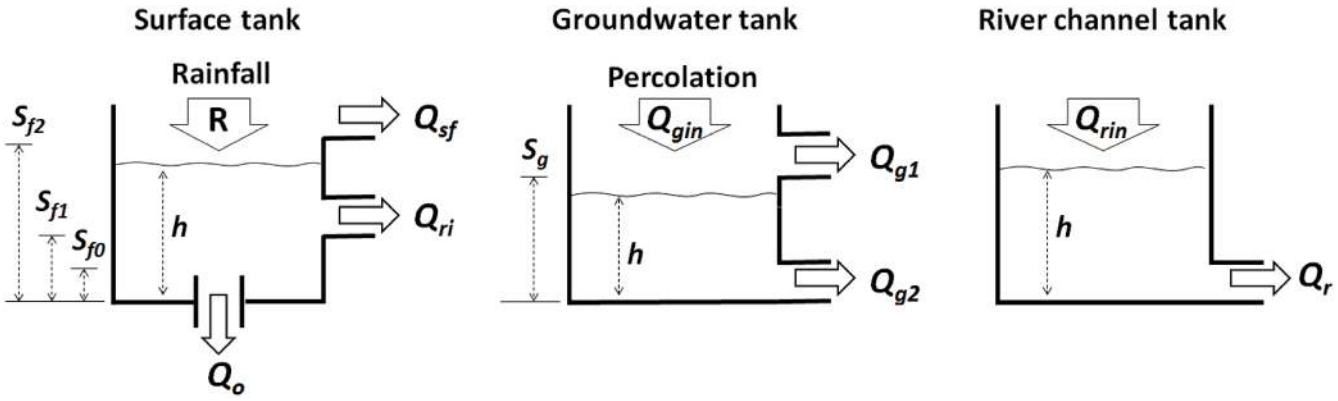

Fig. 3 Schematic diagram of the tank models in the PWRI-distributed hydrological model. Note that $Q_{gin} = Q_o$, $Q_{rin} = Q_{ri}$ or Q_{g2}.

observed rainfall data (ground-based data) at the gauge stations (http://tccip.ncdr.nat.gov.tw/NCDR/main/index.aspx) was used for the rainfall input data. The rainfall input data was distributed into several divisions of the watershed area using the Thiessen polygon method.

2.3 Indicators for the Model Error Analysis

For the quantitative evaluation for the IFAS performance in a past regional flooding event, the root mean square error (RMSE) was used to compute reproducibility (R_p, %) of the simulation result against the observed flood discharge, which is a similar measure of the total water valance error (Fukushima 1988; Sato et al. 2012). The equation is given by

$$R_p = \left(1 - \frac{\mathrm{RMSE}_{MC}}{\mathrm{RMSE}_M}\right) \times 100 \tag{9}$$

where

$$\mathrm{RMSE}_{MC} = \left\{\frac{1}{n_e}\sum_{j=1}^{ne}[Q_M(j) - Q_C(j)]^2\right\}^{1/2} \tag{10}$$

with Q_M is the observed discharge (cms), Q_C is the simulated discharge (cms), n_e is the number of data, and RMSE_M is the error between the observed discharge and zero discharge. The similar evaluation indicator, Nash-Sutcliffe coefficient (Nash and Sutcliffe 1970), is given by

$$NS = 1 - \frac{\sum_{j=1}^{ne}[Q_M(j) - Q_C(j)]^2}{\sum_{j=1}^{ne}[Q_{AVG}(j) - Q_C(j)]^2} \tag{11}$$

where Q_{AVG} is the average discharge for the observation (cms).

Moreover, the quantitative evaluation utilized statistic error analyses: the wave shape error (E_w), volume error (E_v) and discharge-peak error (E_p) (JICE 2001; Aziz and Tanaka 2011). There error are given respectively by

$$E_w = \frac{1}{n_e}\sum_{j=1}^{ne}\left[\frac{Q_M(j) - Q_C(j)}{Q_M(j)}\right]^2 \tag{12}$$

$$E_v = \frac{\sum_{j=1}^{ne} Q_M(j) - \sum_{j=1}^{ne} Q_C(j)}{\sum_{j=1}^{ne} Q_M(j)} \tag{13}$$

$$E_p = \frac{Q_{MP} - Q_{CP}}{Q_{MP}} \tag{14}$$

where Q_{MP} is the peak value of the observed discharge (cms), and Q_{CP} is the peak value of the simulated discharge (cms).

2.4 Sharpness Evaluation for a Distribution

Kurtosis (K_t) is introduced to measure the sharpness of a temporal rainfall distribution obtained from MRI-WRF data or discharge simulated by IFAS. K_t is a measure of whether the data profile has a flat or sharp peak and is given by

$$K_t = \frac{1}{n}\sum_{i=1}^{n}(X_i - \overline{X})^4 \Big/ \left[\frac{1}{n}\sum_{i=1}^{n}(X_i - \overline{X})^2\right]^2 - 3 \tag{15}$$

Negative- and positive-K_t indicate that the peak is flatter and sharper, respectively, against the normal distribution with zero mean and unity variance, $N(0, 1)$. However, it is less effective to compare the sharpness among the distributions different from the normal distribution because a value of K_t shows a relative gap from $N(0, 1)$. We are interested in only the degree of sharpness among any kind of distributions.

3. STUDY SITE

The Tsengwen Reservoir watershed is located in Southern Taiwan (23°20', 120°40'), covering parts of Chiayi County, Tainan County and Kaohsiung County. It is the upper region of the Tsengwen creek watershed. The Tsengwen Reservoir watershed area is approximately 481 km^2, surrounded partly by plateau areas and higher mountains, ranging from 233 to 2609 m in height with a mean slope of approximately 0.54 (Fig. 4). There are two rainfall gauge stations and one discharge gauge station in the watershed (Fig. 4a). The watershed involves a part of the Tsengwen River (138500 m long) and the Tsengwen Reservoir, which is the largest in Taiwan and is the major water supply source for the downstream irrigation system in Chiayi County and Tainan County. The Tsengwen Reservoir has a capacity of approximately 0.5 billion m^3 and has three flood control spillways (9470 cms maximum capacity total) and two outlet channels (150 cms). The annual mean inflow to the reservoir is 1080 million m^3 (e.g., WRA 2004). The mean annual air temperature and precipitation are approximately 19°C and 2700 mm, respectively (Tung 2001). For the IFAS computational conditions in this study, the maximum size of the watershed is 91 × 96 cells (horizontal and vertical) and each cell size is uniform with 400 × 400 m (Fig. 4b). The computational domain is such a small watershed that there is no similar study implemented by the IFAS. For the determination of all parameters in the PWRI-distributed hydrological model, the default values (Table 1) were finally employed after manually tuning with an accepted-value range for each parameter.

4. HYDROLOGICAL MODEL VALIDATION

For the model verification the IFAS was applied to the Tsengwen Reservoir watershed for a severe typhoon event (Typhoon Sinlaku in September 2008), with a strong peak discharge in the temporal distribution (http://ncdr.nat.gov.tw/). The typhoon stalled over north Taiwan and then caused serious damage due to landslides and floods caused by heavy precipitation in the entire Taiwan area (> 1000 mm accumulated rainfall, observed at many gauges). The measured accumulated rainfall and total discharge volume were approximately 750 mm and 0.29 billion m^3, respectively, at the gauges near Tsengwen Reservoir (WRA 2008). Although some GIS-based satellite rainfall data sets (e.g., Global Satellite Mapping of Precipitation, so-called GSMaP_NRT, http://sharaku.eorc.jaxa.jp/GSMaP_crest/, whose resolution is 0.1° for space and 1 hour for time) are available in the IFAS, our watershed area is too small to be appropriately applied to the satellite data spatial resolution. The ground-based observed data for rainfall, one of the options of the IFAS input requirement, was employed (see the locations in Fig. 4 which were averaged over the upper stream area to show the hyetograph

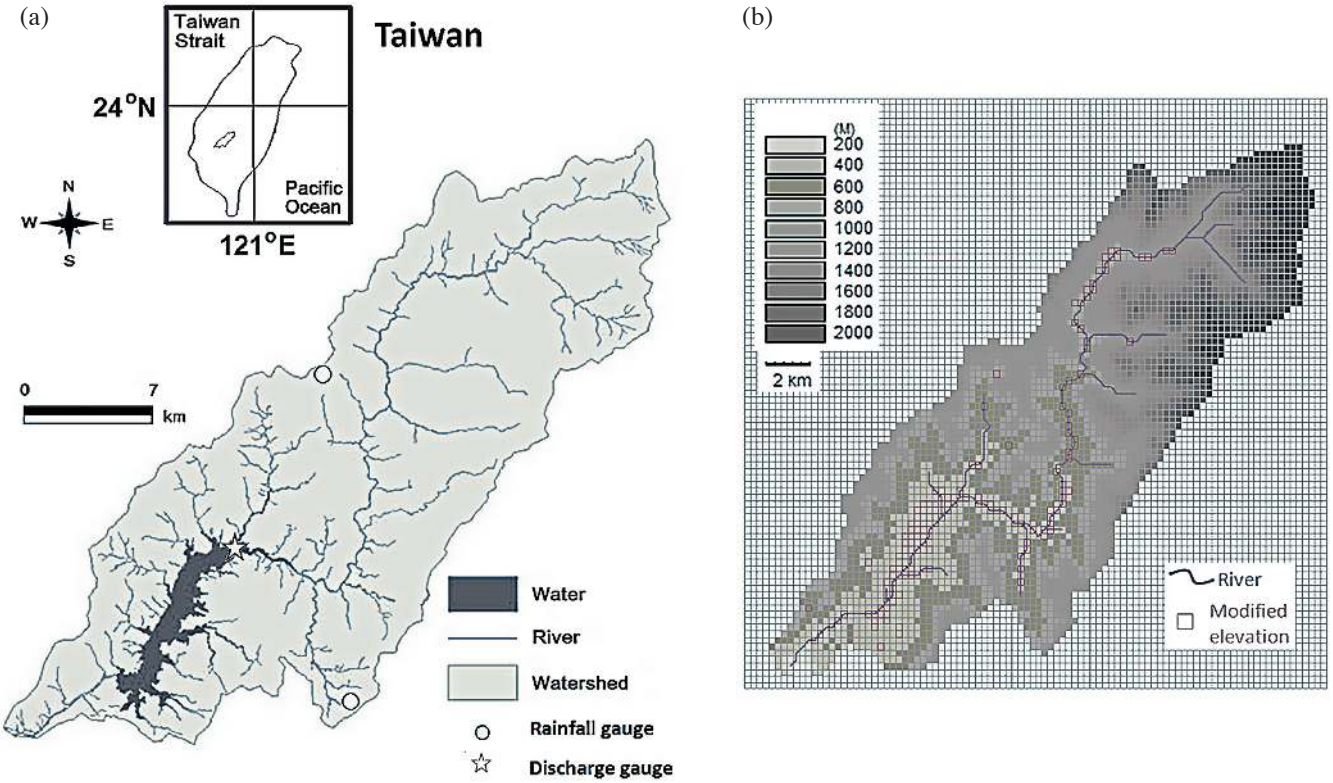

Fig. 4. Map of Tsengwen Reservoir watershed (a), and model grid (b).

Table 1. Default values for the parameters in each tank model.

	Surface tank	Groundwater tank	River tank
Final infiltration capacity (f_0, ms^{-1})	1×10^{-8} - 5×10^{-6}	-	-
Maximum storage height (S_{f2}, m)	0.001 - 0.1	-	-
Height where rapid intermediate outflow occurs (S_{f1}, m)	0.0005 - 0.01	-	-
Height where underground infiltration occurs (S_{f0}, m)	0.0001 - 0.005	-	-
Surface roughness coefficient (n, $m^{-1/3}s$)	0.1 - 2.0	-	-
Regulation coefficient of rapid intermediate outflow (α_{ri})	0.5 - 0.9	-	-
* Initial storage height of surface tank (HIFD, m)	0.0	-	-
Regulation coefficient of slow intermediate outflow (α_u, $m^{-1/2}s^{-1/2}$)	-	0.011	-
Coefficient of base outflow (α_g, s^{-1})	-	3.5×10^{-8}	-
Height where slow intermediate outflow occurs (S_g, m)	-	2.0	-
* Initial storage height of groundwater tank (m, HIGD)	-	2.0	-
Constant of the Resume Law (c)	-	-	7.0
Constant of the Resume Law (s)	-	-	0.5
Manning roughness coefficient of channel (n', $m^{-1/3}s$)	-	-	0.035
* Initial water table of river channel (m, RRID)	-	-	0.2
* Infiltration of aquifer tank (s^{-1}, RGWD)	-	-	0.0
* Coefficient of cross shape (RHW)	-	-	9999.0
* Coefficient of cross shape (RHS)	-	-	1.0
* Coefficient of cross shape (RBH)	-	-	0.5
* Coefficient of cross shape (RBET)	-	-	0.05
* Coefficient of cross shape (RLCOF)	-	-	1.4

*Note: *: These coefficients are internal parameters in the program. Note that the range of some parameters depends on the classification of each tank's characteristics. For example, the Surface tank land use has several categories, such as reservoir, forest, farm land etc.*

in Fig. 5). The discharge simulation with the IFAS was conducted for approximately four days, which was extended due to the discharge time lag against the rainfall input. As seen in Fig. 5 the simulated hydrograph at the gauge station shows a good agreement with the observed one with a reproducibility (R_p) of approximately 74%, as computed by the RMSE analysis in Eq. (9), however the simulated sharp peaks were slightly lower and smoother. The Nash-Sutcliffe coefficient (*NS*) was 0.87 in Eq. (11). Using Eqs. (12), (13), and (14), the quantitative evaluations for the simulated discharge show that $E_w = 0.14$, $E_v = 0.22$, and $E_p = 0.28$, respectively. Those results are approximately equivalent to or acceptable as related to previous studies (Aziz and Tanaka 2011; Wang and Xu 2011; Sato et al. 2012). Therefore, our result implies that the IFAS can provide a reasonable prediction for flood discharge in the Tsengwen Reservoir watershed.

5. RESULTS AND DISCUSSION

We used three terms (Present, Near-future and Future) to simulate the discharge peaks in the upstream river and at the reservoir outlet under climate change. Realistic rainfall time-series were generated by the WRF for the top ten rainfall events for each term. The discharge hydrographs at the gauge station are shown in Fig. 6 for the largest rainfall event for each of the three terms, again with the rainfall data averaged over the upper watershed area. The peak discharge of the Near-future and Future terms increased by a factor of 1.59 and 1.77 times, respectively, compared to the Present term, likely due to the effect of global climate change. The peak of the Future term (approximately 11000 cms) is greater than the maximum dam spillway capacity. Therefore, the dam would need to be operated carefully in order to avoid major flooding downstream.

Figure 7 shows the relation between the discharge peak ratios of the Near-future and Future terms against the Present term for the top ten extreme rainfall events (i.e., the largest rainfall volumes); the figure illustrates how much the ratios of the discharge peak in the future are elevated as compared to the Present peak. Note that the simulated discharge peak

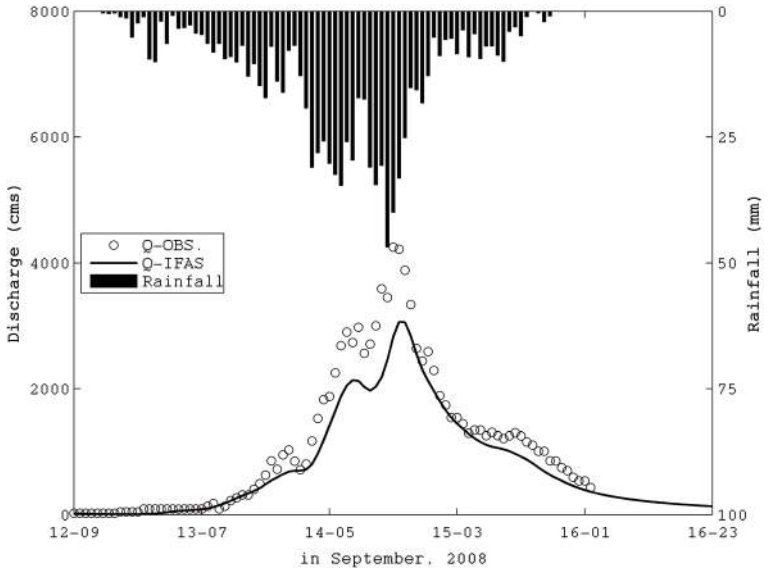

Fig. 5. Hydrograph at the discharge gauge station and rainfall hyetograph, averaged over the upper stream area. The date and time notation (in x axis) shows day-hour.

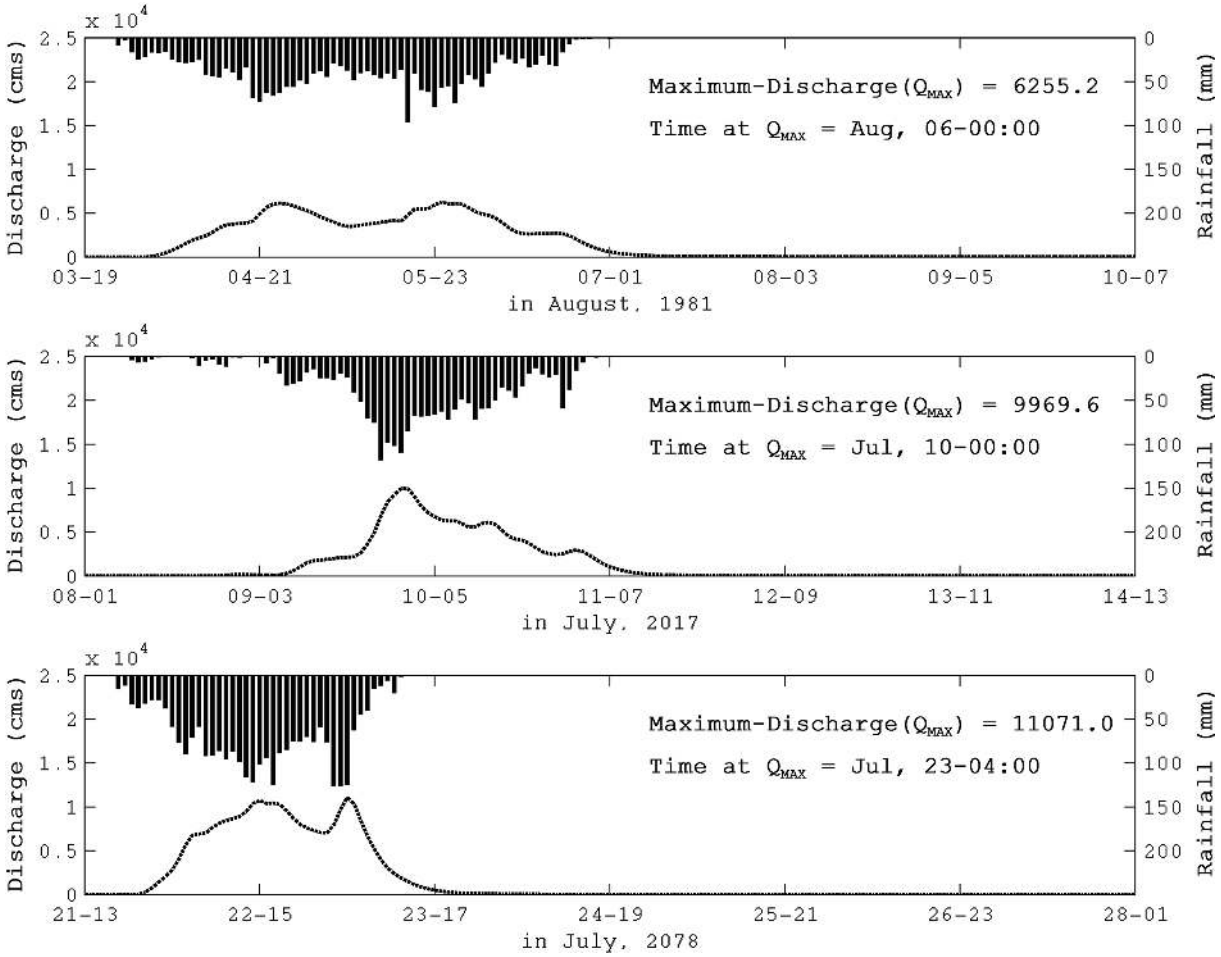

Fig. 6. Discharge hydrograph for the largest rainfall event among three periods: Present (upper), Near-future (middle), and Future (lower) terms. The date and time notation shows day-hour.

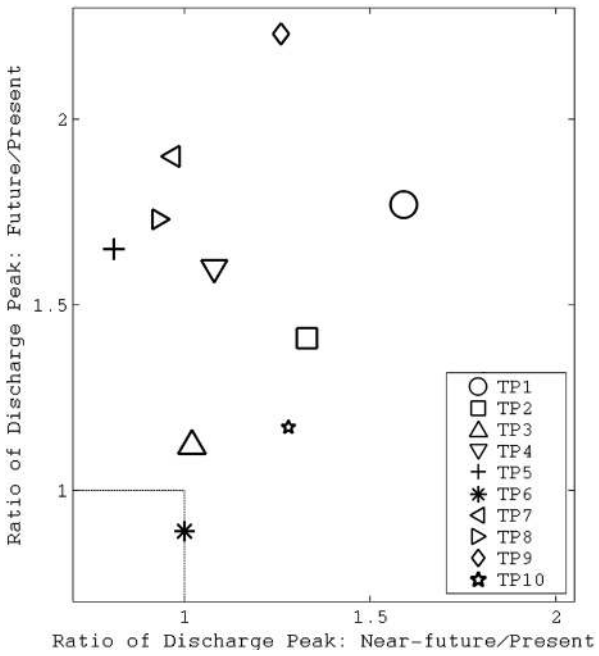

Fig. 7. Discharge peak ratio of the Near-future and Future terms to the Present term for ten rainfall events, TP 1 to TP 10. Note that the dotted lines show a ratio of 1.0 on both axes.

for the top rainfall event is named TP 1 and likewise the tenth largest rainfall event is named TP 10. TP 1, TP 2, and TP 10 peaks have similar ratios of Near-future/Present and Future/Present and these ratios are greater than 1.0. TP 9 has the largest Future/Present discharge peak ratio of 2.23. The peaks of TP 4, TP 5, TP 7, and TP 8 for the Future term are raised by 1.60 to 1.90 times over the Present peak, but the Near-future peaks for these events are approximately similar to those of the Present peak. The TP 3 and TP 6 peaks for both the Near-future and Future terms did not increase as much as compared to the Present term (Table 2). Although the top ten extreme rainfall events were determined by the amount of accumulated rainfall volume, the ranking of rainfall volume for a certain event is not always consistent with its peak discharge ranking. The reason is possibly explained by two factors: discharge volume and distribution shape. Regarding the slope of the discharge distribution that likely affects the maximum peak discharge, the kurtosis (K_t) can be an indicator that shows how much the degree of slope is strong numerically. For example, for the TP 6 peaks among the three terms in Table 3, K_t values indicate that the Present term distribution is sharpest, the Future distribution is more flat and the Near-future distribution is between the Present and Future distributions even though the total discharge volume becomes larger as time progresses (i.e., from the Present to Future terms). The Present peak for TP 7 is similar to the Near-future peak because of the flat distribution of the Near-future hydrograph (large negative K_t); the Present peak is lower than the Future peak because these hydrographs had the same K_t value even though the TP 7 volumes of the hydrographs increased in the time series.

Dam drainage facilities are normally able to cut the flood discharge peak depending upon the balance between drainage capacity (e.g., spillway) and net water stored in a reservoir. The net water is the water remaining in the reservoir accounting for appropriate discharge at the dam outlet/spillway facilities that would not exceed the dam spillway capacity or target discharges for downstream communities. Given that peak discharges are expected to be larger in the future, it is necessary to evaluate whether future flood discharges can be stored in the reservoir without causing major downstream flooding. In Fig. 8 the temporal distributions of the total flood discharges entering the reservoir for the top ten rainfall events (i.e., at the dam outlet before accounting for the dam operations to reduced the peak discharges) the Near-future and Future terms are shown along with the maximum dam drainage capability (9620 cms) and the design discharge peak (6900 cms, hereinafter being called a realistic value) of the river downstream of the the reservoir (about 10 km downstream) (Yeh et al. 2010). Those values (the maximum and realistic values) are considered a discharge criterion for flood risk management in this study. Hereinafter, the maximum and realistic values are called maximum and realistic criteria. Note that the simulated amounts of discharge at the dam outlet were approximately 28 - 29% greater than at the gauge station due to ungauged areas downstream of the gauge station but upstream of the dam outlet, including direct precipitation on the reservoir surface (the total reservoir drainage area is 30% greater than the watershed upstream of the gauge station).

The temporal discharge distributions of some of the more extreme floods (e.g., TP 1 - TP 3) are greater than the maximum criterion for approximately one day for the Near-future and Future terms. Most discharge distributions for the Near-future term, except for the relatively low ranking floods such as TP 8 and TP 9, are in excess of the design discharge of the river downstream of the dam. The degree of excessive discharge for the Future term is more enhanced compared to the Near-future term. Discharges exceeding the maximum and realistic criteria must be stored in the reservoir.

The net excess water stored in the reservoir was computed by integrating the volume of discharge at each time step (1 h) temporally and subtracting the maximum or realistic criterion at the dam outlet. If the net excess water was negative, it was forced to be zero (i.e., dam releases could not be greater than the total inflow into the reservoir). Based upon the maximum and realistic criteria, the excess waters for the Near-future and Future extreme floods (caused by the top ten extreme rainfall events) are shown in Fig. 9. The net excess water can be compared not only with the total dam capacity but with the flood control capacity (FCC), which is a part of the total capacity and can be thought of as the available volume to regulate and store flood waters except for

agricultural irrigation and drinking water use. In anticipation of a flood the dam operator would release a volume of water from the reservoir equal to the FCC. For the Tsengwen Reservoir, the FCC changes seasonally but remains within upper and lower limits (WRA 2002). Based upon the seasonal variation in the FCC, we determined the upper and lower limits of the FCC during the typhoon season, from June to September (Fig. 9). The values for the upper and lower limits of the FCC are 1.25 and 3.20 × 10^8 (m^3), respectively. For the floods in the Near-future term, the excess water required to

Table 2. Discharge peak ratios for the Near-future and Future terms as compared to the Present term for the top ten rainfall events.

	Near-future/Present	Future/Present
TP 1	1.59 (0.84)	1.77 (1.06)
TP 2	1.33 (0.69)	1.41 (1.00)
TP 3	1.02 (1.13)	1.12 (1.51)
TP 4	1.08 (1.01)	1.60 (1.55)
TP 5	0.81 (1.50)	1.65 (2.12)
TP 6	1.00 (1.50)	0.89 (2.17)
TP 7	0.97 (1.50)	1.90 (1.94)
TP 8	0.93 (1.13)	1.73 (1.72)
TP 9	1.26 (1.22)	2.23 (1.94)
TP 10	1.28 (1.37)	1.17 (2.24)

Note: ( ) shows the ratios for rainfall volume.

Table 3. Features of the discharge distribution for the Present, Near-future and Future terms for the top ten rainfall events.

	Present		Near-future		Future	
	* Vol	* Kurt	Vol	Kurt	Vol	Kurt
TP 1	9.35	-0.97	7.80	-0.40	9.99	-0.80
TP 2	9.04	-0.62	6.27	-0.45	9.15	-0.75
TP 3	5.33	0.07	6.04	-0.56	8.03	-0.39
TP 4	4.92	-1.32	4.98	-0.72	7.77	-0.48
TP 5	3.19	-0.02	4.76	0.04	6.92	0.17
TP 6	2.97	1.48	4.46	0.23	6.56	-0.44
TP 7	2.78	-0.15	4.09	-0.83	5.57	-0.15
TP 8	2.60	-0.58	2.81	-0.67	4.71	0.54
TP 9	2.19	0.30	275	-0.40	455	-0.29
TP 10	1.92	3.51	271	0.36	450	0.11

*Note: *: Vol and Kurt represent the accumulated discharge volume and kurtosis, respectively. Their units are × 10^8 (m^3) and no dimension, respectively.*

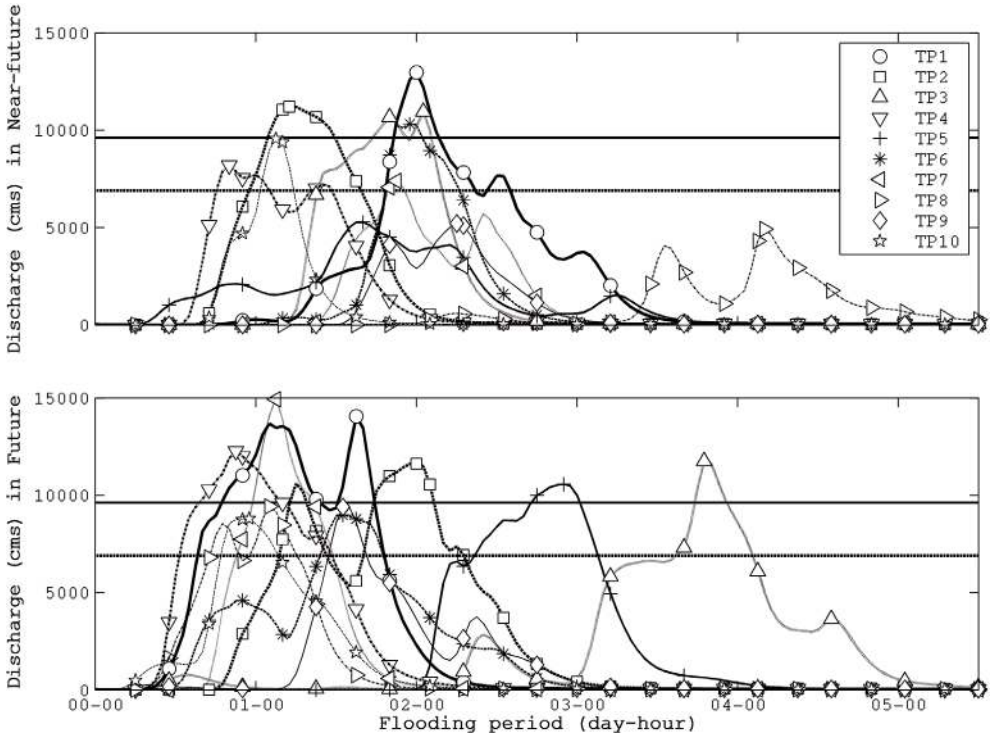

Fig. 8. Temporal distributions of discharge for TP 1 to TP 10 for the Near-future and Future extreme floods, which were before changes in operations of the dam were taken into account to reduce the peak discharge for downstream flood management. Note that thick horizontal solid and dashed lines represent the maximum capacity of the reservoir drainage facilities (i.e., spillways) and the design discharge peak for the communities downstream of the dam, respectively. Note that the upper figure is for the Near-future distributions and the lower for Future distributions.

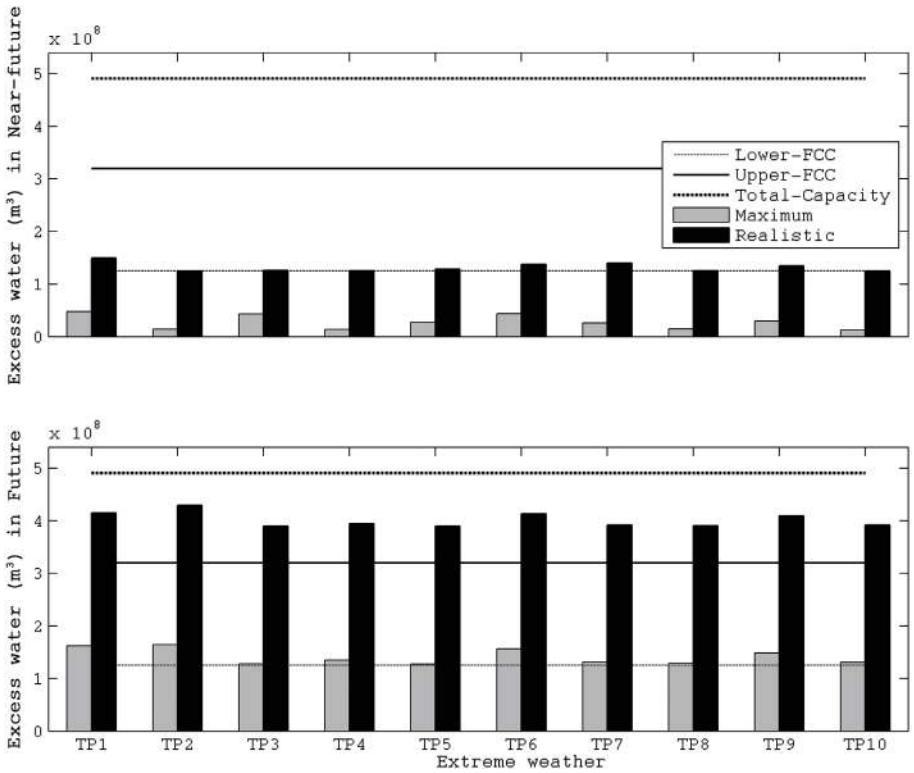

Fig. 9. Net waters stored in the Tsengwen Reservoir during each extreme rainfall event taking into account two different dam outlet scenarios. The grey and black bars indicate the stored water for the maximum criterion of the drainage system (i.e., allowing the maximum discharge from the dam outlet/spillway facilities of 9620 cms) and the stored water of the realistic criterion (i.e., maximum dam releases of 6900 cms to reduce downstream flooding), respectively. The horizontal lines (from top to bottom) indicate the total dam capacity, upper FCC (i.e., flood control capacity) and lower FCC. Note that the upper figure is for the Near-future term and the lower figure is for the Future term.

be stored in the reservoir caused by the maximum criterion take up only 2.7 - 9.7% of the total dam capacity, 4.1 - 14.9% of the upper limit of the FCC, and 10.5 - 38.0% of the lower limit of the FCC, respectively. Therefore, it is expected that there is sufficient total dam capacity and FCC to contain flood discharges in the Near-future term and not exceed the dam spillway capacity (or maximum criterion). However, to maintain the realistic criterion (a discharge of only 6900 cms downstream of the dam) the dam must be carefully operated because Fig. 9 shows that the excess water could be up to 20% greater than the lower FCC limit.

On the other hand, the floods induced by the top ten extreme rainfall events for the Future term may cause a severe problem for flood control operations because the excess water volume would be over 1.2 - 3.4 times the lower limit of the FCC and 1.2 - 1.3 times the upper limit of the FCC under the realistic criterion. In particular, the excess water volume is stored with 79.6 - 87.5% of the total dam capacity under the realistic criterion, or in other words the reservoir would need to be almost empty prior to the event in order to store the flood waters. These results suggest that floods in the Future term may cause severe inundation damage in the downstream region if stored water in the reservoir is not released from the dam before an extreme rainfall event occurs. Therefore, extreme care will be needed to handle dam releases for flood control for the Future term.

However, as a further consideration of this work, it is necessary to take into consideration the impact of accumulated sediment on the reservoir storage capacity for a severe flood in the future. For instance, Typhoon Morakot (August 2009) brought 91 million m^3 of accumulated sediment into the Tsengwen Reservoir, resulting in a 22.3% reduction in storage capacity (Yang et al. 2010). The sedimentation effect on the reservoir capacity is beyond the scope of this study.

6. CONCLUSION

We implemented a hydrological model (IFAS) programmed to a local watershed in Taiwan to better estimate future flood characteristics under global climate change. This study focused on simulating discharge peaks for extreme rainfall events in order to understand the implications for dam operations and flood control. The rainfall data under climate change for three terms (Present, Near-future and Future) were projected using the regional climate model (i.e., WRF), driven by the MRI-AGCM3.2S. IFAS verification was first conducted using a past flood event (Typhoon Sinlaku). The simulated discharge was in good agreement with

the observed (74% reproducibility). A simulation of flood discharge under the top ten rainfall events, based upon their volumes and named TP 1 to TP 10, for each term was projected by the WRF with a 5 km resolution. The results show that the peak discharge ranking was not consistent with the total rainfall volume ranking due to different simulated discharge hydrograph shapes (i.e., temporal distribution). Specifically, the ratios of the discharge peak for the Near-future/Present and Future/Present for TP 1, TP 2, TP 9, and TP 10 indicate that the Near-future and Future flood peaks were more severe than the Present peaks. In addition, the Future peaks for TP 4, TP 5, TP 7, and TP 8 were higher than those for the Present peaks. Finally, to understand the climate change effect on the reservoir's flood control purposes, the balance between the floodwater stored in the reservoir and the water discharged from the dam spillways was evaluated. For Future floods it may be necessary to release discharges from the dam outlet in excess of the design discharge peak, which is aimed at minimizing downstream damage or the reservoir must be drawn down before severe typhoons arrive more than the current upper limits for the FCC and possibly even to almost the total dam capacity.

Acknowledgements We are grateful for the IFAS package from Dr. Fukami Kazuhiko of ICHARM, the MRI data from Dr. Akio Kitoh of the Japan Meteorological Research Institute, the assistance from Ms. Huei-Syuan Fu (NCDR) and the helpful comments from the editor and the Anonymous Reviewers. We deeply appreciate the financial support from the Taiwan National Science Council (NSC 100-2621-M-492-001) and from the SOUSEI Program of the Ministry of Education, Culture, Sports, Science and Technology of Japan.

REFERENCES

Aziz, A. and S. Tanaka, 2011: Regional parameterization and applicability of integrated flood analysis system (IFAS) for flood forecasting of Upper-Middle Indus River. *Pakistan J. Meteorol.*, **8**, 21-38.

Bernstein, L., P. Bosch, O. Canziani, Z. Chen, R. Christ, O. Davidson, W. Hare, S. Huq, D. Karoly, V. Kattsov, Z. Kundzewicz, J. Liu, U. Lohmann, M. Manning, T. Matsuno, B. Menne, B. Metz, M. Mirza, N. Nicholls, L. Nurse, R. Pachauri, J. Palutikof, M. Parry, D. Qin, N. Ravindranath, A. Reisinger, J. Ren, K. Riahi, C. Rosenzweig, M. Rusticucci, S. Schneider, Y. Sokona, S. Solomon, P. Stott, R. Stouffer, T. Sugiyama, R. Swart, D. Tirpak, C. Vogel, G. Yohe, R. K. Pachauri, and A. Reisinger, 2007: Climate Change 2007: Synthesis Report, Contribution of Working Groups I, II and III to the Fourth Assessment Report of the Intergovernmental Panel on Climate Change, IPCC, Geneva, Switzerland, 104 pp.

Field, C. B., V. Barros, T. F. Stocker, and Q. Dahe, 2012: Managing the Risks of Extreme Events and Disasters to Advance Climate Change Adaptation: Special Report of the Intergovernmental Panel on Climate Change, Cambridge University Press, Cambridge, New York, USA, 592 pp.

Fukami, K., Y. Sugiura, J. Magome, and T. Kawakami, 2009: Integrated Flood Analysis System (IFAS Ver. 1.2), User's Manual. Japan PWRI-technical note, No.4148, 223 pp.

Fukushima, Y., 1988: A model of river flow forecasting for a small forested mountain catchment. *Hydrol. Process.*, **2**, 167-185, doi: 10.1002/hyp.3360020207. [Link]

Hsu, M. H., J. C. Fu, and W. C. Liu, 2003: Flood routing with real-time stage correction method for flash flood forecasting in the Tanshui River, Taiwan. *J. Hydrol.*, **283**, 267-280, doi: 10.1016/S0022-1694(03)00274-9. [Link]

Hsu, H. H., C. Chou, Y. Wu, M. M. Lu, C. T. Chen, Y. M. Chen, 2011: Climate Change in Taiwan: Scientific Report 2011 (Summary), National Science Council, Taipei, Taiwan, 67 pp.

Houghton, J. T., G. J. Jenkins, and J. J. Ephraums, 1990: Climate Change: The IPCC Scientific Assessment, Cambridge University Press, Cambridge, United Kingdom, 416 pp.

Houghton, J. T., L. G. M. Filho, J. P. Bruce, H. Lee, B. A. Callander, and E. F. Haites, 1995: Climate Change 1994: Radiative Forcing of Climate Change and An Evaluation of the IPCC IS92 Emission Scenarios, Cambridge University Press, Cambridge, United Kingdom, 347 pp.

Japan Institute of Construction Engineering (JICE), 2001: Outflow analysis system, analytical technique manual Ver2.3, last accessed, Dec, 2013. Available at http://www.jice.or.jp/.

Kitoh, A., A. Yatagai, and P. Alpert, 2008: First super-high-resolution model projection that the ancient "Fertile Crescent" will disappear in this century. *Hydrol. Res. Lett.*, **2**, 1-4, doi: 10.3178/hrl.2.1. [Link]

Mizuta, R., K. Oouchi, H. Yoshimura, A. Noda, K. Katayama, S. Yukimoto, M. Hosaka, S. Kusunoki, H. Kawai, and M. Nakagawa, 2006: 20-km-Mesh global climate simulations using JMA-GSM model -Mean Climate States-. *J. Meteorol. Soc. Jpn.*, **84**, 165-185, doi: 10.2151/jmsj.84.165. [Link]

Mizuta, R., H. Yoshimura, H. Murakami, M. Matsueda, H. Endo, T. Ose, K. Kamiguchi, M. Hosaka, M. Sugi, S. Yukimoto, S. Kusunoki, and A. Kitoh, 2012: Climate simulations using MRI-AGCM3.2 with 20-km grid. *J. Meteorol. Soc. Jpn.*, **90A**, 233-258, doi: 10.2151/jmsj.2012-A12. [Link]

Nash, J. E. and J. V. Sutcliffe, 1970: River flow forecasting through conceptual models part I - A discussion of principles. *J. Hydrol.*, **10**, 282-290, doi: 10.1016/0022-1694(70)90255-6. [Link]

National Science and Technology Center for Disaster Reduction (NCDR), 2010: Introduction of Taiwan Climate Change Projection and Information Platform Project (TCCIP), NCDR report 2010-54, 7 pp. (in Chinese)

Oouchi, K., J. Yoshimura, H. Yoshimura, R. Mizuta, S. Kusunoki, and A. Noda, 2006: Tropical cyclone climatology in a global-warming climate as simulated in a 20 km-Mesh global atmospheric model: Frequency and wind intensity analyses. *J. Meteorol. Soc. Jpn.*, **84**, 259-276, doi: 10.2151/jmsj.84.259. [Link]

Piani, C., J. O. Haerter, and E. Coppola, 2010: Statistical bias correction for daily precipitation in regional climate models over Europe. *Theor. Appl. Climatol.*, **99**, 187-192, doi: 10.1007/s00704-009-0134-9. [Link]

Sato, Y., T. Kojiri, Y. Michihiro, Y. Suzuki, and E. Nakakita, 2012: Estimates of climate change impact on river discharge in Japan based on a super-high-resolution climate model. *Terr. Atmos. Ocean. Sci.*, **23**, 527-540, doi: 10.3319/TAO.2012.05.03.02(WMH). [Link]

Sugiura, T., K. Fukami, and H. Inomata, 2008: Development of Integrated Flood Analysis System (IFAS) and its applications. World Environmental and Water Resources Congress 2008, 1-10, doi: 10.1061/40976(316)279. [Link]

Tung, C. P., 2001: Climate change impacts on water resources of the Tsengwen creek watershed in Taiwan. *J. Am. Water Resour. Assoc.*, **37**, 167-176, doi: 10.1111/j.1752-1688.2001.tb05483.x. [Link]

Wang, G. and Z. Xu, 2011: Assessment on the function of reservoirs for flood control during typhoon seasons based on a distributed hydrological model. *Hydrol. Process.*, **25**, 2506-2517, doi: 10.1002/hyp.8023. [Link]

Water Resources Agency (WRA), 2002: Appendix-2 - Main Point for the Water Control Operation in Tsengwen Reservoir (2013 updated version). Republic of China Ministry of Economic Affairs. (in Chinese)

Water Resources Agency (WRA), 2004: Hydrological Year Book of Taiwan. Republic of China Ministry of Economic Affairs. (in Chinese)

Water Resources Agency (WRA), 2008: Disaster report for Typhoon Sinlaku. Water conservancy emergency experiential learning center, Republic of China Ministry of Economic Affairs.

Yang, W. F., C. S. Yeh, S. Y. Lien, P. C. Hou, C. R. Huang, M. C. Lee, and Y. T. Lee, 2010: Discussion on Issues of Tseng-Wen Reservoir Transbasin Water Diversion Project After Typhoon Morakot. *Sino-Geotechnics*, **126**, 29-38. (in Chinese)

Yen, C. L., T. H. Lee, R. Y. Wang, D. L. Yang, and M. H. Hsu, 1998: Research and Development of Flood Forecasting System Model for Tanshui River Basin, Technical Report. Republic of China Ministry of Economic Affairs. (in Chinese)

Yeh, C. L., S. H. Yang, S. T. Wei, T. C. Hsieh, 2010: Review and Application of the River Warning Level and the Regional Drainage Alert by Rainfall. Water Resources Agency, Republic of China Ministry of Economic Affairs. (in Chinese)

Yoshino, F., J. Yoshitani, and M. Sugiura, 1990: A conceptual distributed model for large-scale mountainous basins. In: Lang, H. and A. Musy (Eds.), Hydrology in Mountainous Regions. I - Hydrological Measurements; the Water Cycle, No. 193, 685-692, IAHS, Lausanne, Switzerland.